

How turbulence increases the bubble-particle collision rate

Linfeng Jiang¹ and Dominik Krug^{1,*}

¹*Physics of Fluids Group, Max Planck Center Twente for Complex Fluid Dynamics and Johannes Martinus Burgers Centre for Fluid Dynamics, University of Twente, 7500 AE Enschede*

(Dated: July 3, 2024)

Abstract

We study the effect of turbulence on collisions between a finite-size bubble and small inertial particles based on interface-resolved simulations. Our results show that the interaction with the flow field around the bubble remains the dominant effect. Nonlinear dependencies in this process can enhance the turbulent collision rate by up to 100% compared to quiescent flow. Fluctuations in the bubble slip velocity during the interaction with the particle additionally increase the collision rate. We present a frozen-turbulence model that captures the relevant effects providing a physically consistent framework to model collisions of small inertial particles with finite-sized objects in turbulence.

Introduction.—Bubble-particle collisions are central to the flotation process, which is widely used e.g. in the mining industry to separate minerals through their attachment to rising bubbles. This intricate process involves a wide range of colloid science disciplines[1–3] with significant complexity stemming from the interplay of hydrodynamics and physicochemical interactions. The hydrodynamic bubble-particle interaction remains of paramount importance for optimization, as it is the rate-determining step that also sets the conditions for other interactions.

Most of the work on bubble-particle col-

lisions draws on the large body of work on particle-particle collisions [4], in particular the seminal work of [5] for the tracer limit and the model proposed by [6] for the kinetic gas limit at large particle inertia. Such models predict the collision rate without considering the hydrodynamic interaction between the collision partners, but must take into account effects such as the segregation of bubbles and particles in a turbulent flow[7, 8]. However, the significant size difference between the larger bubble and the mineral particles in a typical flotation process, makes it important to account for the flow distortion around the bubble. This can cause an

* d.j.krug@utwente.nl

encountering particle to be deflected, reducing the actual number of collisions. For a bubble rising in quiescent flow, this process is deterministic and has been widely studied [2, 9–16]. In this case, the effect of the hydrodynamic interaction can be captured in terms of collision efficiency, which relates the rate of actual collisions to the encounter rate. The lack of a suitable concept to account for turbulence in this context is widely acknowledged in the literature [17–19]. Existing approaches are flawed because they combine turbulent encounter rates with collision efficiencies applicable to pure gravitational settling [20–25]. Others use a Reynolds-type decomposition, which is problematic given the strongly nonlinear dependence of the problem on the flow velocity. Another conceptual inconsistency is that the encounter rate is based on the bubble-particle relative velocity, whereas the collision efficiency is determined by the bubble slip relative to the fluid. Some of these deficiencies are overcome in the model of Refs. [26, 27], which however remains limited to tracer particles.

The core problem is to determine the collision rate of small inertial particles with a finite-size object in a turbulent flow. This is of general relevance to many other applications beyond flotation, such as the collision of cloud droplets [28, 29], the accretion of planetesimals by the collection of dust particles

[30, 31], depth filtration [32, 33], or bacterial degradation of marine snow [34, 35]. However, the scarcity of data due to the difficulties in performing the necessary experiments and interface-resolved simulations, has hindered the progress of theoretical research in this area.

In this Letter, we present a combined numerical and theoretical study of the effects of turbulence on bubble-particle collisions using state-of-the-art direct numerical simulations. We adopt homogeneous and isotropic turbulence (HIT), in which we measure how turbulent fluctuation modifies the bubble-particle collision rate along the bubble-rising path. The turbulent flow is characterized by the Taylor Reynolds number, $Re_\lambda \equiv \sqrt{15u'}/(\nu\epsilon)$, where u' denotes the root-mean-square velocity of the turbulence, ν is the kinematic viscosity, and ϵ is the mean kinetic energy dissipation rate. The bubble dynamics are governed by the bubble Reynolds number $Re_b = 2r_b\overline{U}_b/\nu$, where \overline{U}_b is the average bubble rising velocity and r_b denotes the bubble radius, and by the turbulence intensity $T_i = u'/\overline{U}_b$.

Model.—The collision rate K of particles with a bubble is determined by $K = \Gamma n_p$, where n_p is the particle number density and the proportionality coefficient Γ (m^3s^{-1}) is commonly referred to as the collision kernel and is determined by the flow [4]. In quies-

cent flow, the behaviour is deterministic and the particle grazing trajectory Ψ_c determines a stream tube for which all the particles contained inside collide with the bubble. Far enough upstream of the bubble, the grazing trajectory leads to a critical radius r_c , as illustrated in Fig. 1(a). Thus, the collision kernel in quiescent flow can be expressed as $\Gamma_q = \pi r_b^2 U_b E_c$. Here $E_c = r_c^2/r_b^2$ denotes the collision efficiency [15, 16], which depends on Re_b , the bubble-particle size ratio r_p/r_b and the Stokes number $St_p = \tau_p/\tau_f$, with τ_p the particle response time and $\tau_f = 2r_b/U_b$ the timescale of the bubble-particle interaction.

To provide an understanding of the relevant physical mechanisms, we propose a statistical model. We start from the assumption that the flow field in the vicinity of the bubble is approximately stationary and uniform during the bubble-particle interaction. This implies that the temporal scale τ_f is shorter than the correlation timescale of flow fluctuations ($O(\tau_\eta)$). Additionally, the flow correlation length scale (10η) should be comparable or larger than the bubble size. Within this ‘frozen turbulence’ assumption, the instantaneous bubble-particle collision process in turbulence can be related back to that observed in quiescent flow. The equivalent steady flow problem is characterised by the magnitude of the instantaneous bubble slip velocity U'_b with corresponding values of $Re'_b = Re_b U'_b/\bar{U}_b$

and $St'_p = St_p U'_b/\bar{U}_b$.

The entire bubble-particle collision process in a turbulent flow can then be viewed as a superposition of collision events in quiescent flow with varying parameters Re'_b and St'_p . Based on this, the collision kernel can be derived as follows [36]:

$$\Gamma = \frac{K}{n_p} = \frac{\pi r_b^2}{n_p} \int E_c(Re'_b, St'_p) U'_b f(U'_b) n'_p dU'_b. \quad (1)$$

where the local instantaneous particle number density n'_p is introduced to account for fluctuations in this quantity upstream of the bubble. Importantly $E_c(Re'_b, St'_p)$ denotes the collision efficiency in quiescent flow for varying flow parameters, which is deterministic and can be parameterised. The collision kernel is therefore determined by the probability density function (PDF) $f(U'_b)$ of the bubble slip velocity U'_b , which is the main input to the model.

Interface-resolved simulations.—For the simulations to test this model, we use a code based on the lattice Boltzmann method (LBM) to solve the Navier-Stokes equations [37], which has been employed before to study dynamics of point-like [38–40] and finite-size particles [41, 42] in turbulence. We assume the bubble to be fully contaminated with a no-slip boundary condition, spherical and non-deformable. The coupling between the contaminated bubble and

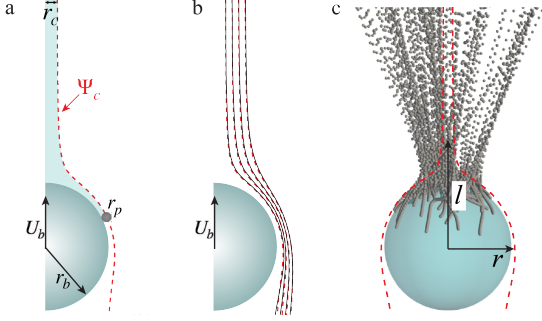


FIG. 1. (a) Sketch of the grazing trajectory (red dashed line) in quiescent flow. (b) Mean flow streamlines around the bubble in HIT (solid) and quiescent flow (dashed lines). (c) Trajectories of colliding particles ($r_p/r_b = 0.05$, $St_p = 0.04$) in HIT compared to the corresponding grazing trajectories (red lines) in quiescent flow at the same $Re_b = 120$.

the flow is resolved by the immersed boundary method[43–45]. Two sets of simulations are carried out[36]: 1) a simplified configuration where a constant bubble velocity is imposed, and 2) simulations with a freely rising bubble, where the bubble-fluid density ratio is 10^{-3} . Matching practically relevant conditions[46], we consider a moderately turbulent flow ($Re_\lambda = 32$ and 64) and a bubble Reynolds number $Re_b \sim O(100)$. Additionally, we conduct simulations of bubble-particle collisions in a quiescent flow at Re_b ranging from 80 to 210. In the flotation process, the mineral particles are significantly smaller than the turbulent dissipation scale η . We represent these as one-way coupled

point particles[36], considering the drag force and the added mass force. The particle response time $\tau_p = r_p^2/(3\beta\nu)$ includes the density ratio $\beta = 3\rho_f/(\rho_f + 2\rho_p)$, where ρ_f and ρ_p denote the density of the fluid and the particle, respectively. Note that the ratio of turbulent dissipative time scale τ_η to τ_f in our simulations is $\sim O(1)$. The collision rate, $K = N_c/T$ and thus the collision kernel $\Gamma = K/n_p$, is measured by counting the number of particles (N_c) that collide with the bubble over a time period T .

Imposed bubble velocity.—We start from the discussion of the bubble with an imposed velocity. In Fig. 1(b) we demonstrate that the impact of turbulent fluctuations on the mean streamlines is insignificant for the present parameters. In particular in the incoming flow, which determines the collision rate, the differences are very small, lending support to our modelling approach. More noticeable differences in the wake region are a consequence of turbulence disrupting the symmetric recirculation pattern behind the bubble. However, the influence of turbulence on the collision process is distinct, as becomes evident from the movie [36] and Fig. 1(c), where trajectories of colliding particles are shown. These trajectories originate from a cone-shaped region that is notably larger than the corresponding collision radius r_c , based on the grazing trajectory in

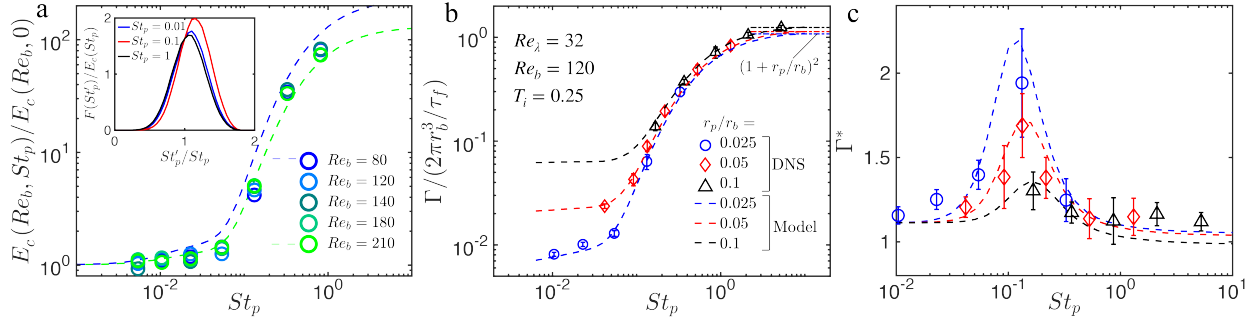


FIG. 2. (a) Normalised E_c as a function of St_p in quiescent flow for various Re_b compared to the fits according to Eq. (2) (dashed lines). Inset: scaled PDF of St'_p as a function of St'_p for different St_p . (b) Dimensionless collision kernel vs. St_p at $Re_b = 120$ for bubble with imposed velocity in HIT (symbols) and model (dashed lines). (c) Turbulent collision kernel relative to that in quiescent flow for the imposed velocity bubble. Error bars represent fluctuations between subsets of the data.

quiescent flow. Correspondingly, also the collision angle relative to the direction of the imposed bubble velocity is found to be wider in the turbulent flow [36]. Nevertheless, the collision trajectories appear to follow straight paths towards the bubble, which is consistent with our modelling assumptions.

For quiescent flow, the dependence of E_c normalised by the result for tracer particles $E_c(Re_b, 0)$, on Re_b and St_p is presented in Fig. 2(a). For small St_p , the inertial effect is negligible and the particles follow the flow streamlines, so that interception is the dominant factor determining the number of collisions in this range [47]. Analytical predictions based on flow streamlines in quiescent flow indicate that Γ scales with $(r_p/r_b)^2$ [14, 48] in this case. However, as particle inertia becomes more pronounced, par-

ticles deviate from the flow streamlines and collide on the bubble even if their initial position is outside the grazing trajectory of the inertialess particle. This leads to a higher collision rate and explains the rapid increase in E_c as St_p approaches 0.1, beyond which the inertial effect dominates. At very large St_p , the particles are barely influenced by the flow such that E_c approaches $(1 + r_p/r_b)^2$. To be able to evaluate $E_c(Re_b, St_p)$ analytically, we employ an empirical expression, which is the sum of its two contributions: interceptional collision E_i and the collision associated with particle inertia [14]:

$$E_c = E_i + \left(1 + \frac{r_p}{r_b}\right)^2 \left(\frac{St_p}{St_p + a}\right)^b \left(\chi - \frac{E_i}{(1 + r_p/r_b)^2}\right) \quad (2)$$

Here, we adopt $E_i = \frac{3}{2}(r_p/r_b)^2(1 + Re_b^{2/3}/5)$ [15] for the collision efficiency in the tracer

limit and the fitting parameters are set to $a = 0.2$ and $b = 2$. $\chi = 1 - 0.9 \cdot 10^{-\left(\frac{\log(St)+1.3}{1.6}\right)^2}$ is a fitting correction term to better capture the transition around $St_p \approx 0.1$. The resulting fit is in good agreement with the data for the evaluated parameter range as shown in Fig. 2(a).

As shown for the case with constant bubble velocity in Fig. 2(b), the general trends of Γ in turbulence, in particular the increase with increasing St_p for all particle sizes are consistent with those observed in quiescent flow. In this simplified configuration, the PDF of the U'_b required to evaluate our model (Eq. 1), can be obtained by combining the constant bubble rise velocity with the Gaussian distribution of turbulent velocity fluctuations [36]. The collision kernel predicted in this way is in excellent agreement with the simulations. This is further confirmed in Fig. 2(c), where we scrutinize the result by plotting it relative to the collision kernel at the same bubble velocity in quiescent flow as $\Gamma^* = \Gamma/\Gamma^q$. In this way, it also becomes clear that turbulent flow significantly enhances the collision kernel. Two interesting aspects should be underscored: Firstly, Γ^* surpasses 1 when inertia is negligible ($St_p \ll 1$), indicating that turbulent fluctuations enhance interceptional bubble-particle collision. Secondly, the collision enhancement is not uniform across the consid-

ered range of St_p , suggesting that the combined influence of turbulence and particle inertia leads to further amplification of the collision rate. The collision enhancement can reach approximately 100% for particles with a size ratio of $r_p/r_b = 0.025$. For larger particles, the maximum collision enhancement is lower, though the peak still occurs at a similar value of $St_p \approx 0.1$.

The good agreement with the simulations indicates that the model adequately captures the relevant turbulence effects on the collisions, enabling us to explore their origin. We notice that due to the increase of E_c with increasing Re'_b , the integrand in Eq. (1) nonlinearly depends on U'_b . This results in an increase in the predicted collision rate even if $f(U'_b)$ is symmetric around \bar{U}_b . In the present case, this effect amounts to close to 15% increase in Γ , consistent with what is observed at low St_p .

In addition, there is an inertial effect as a change in U'_b also changes St'_p . The strongly nonlinear dependence of E_c on St'_p , especially in the intermediate range $St_p \approx 0.1$, leads to an asymmetry response to positive and negative velocity fluctuations. This is demonstrated by the scaled PDF of St'_p , $F(St'_p) = E_c(St'_p)PDF(St'_p)$, shown in the inset of Fig. 2(a). For low and high St_p , the dependence of $F(St'_p)$ on St'_p is almost symmetric. However, for an intermediate value

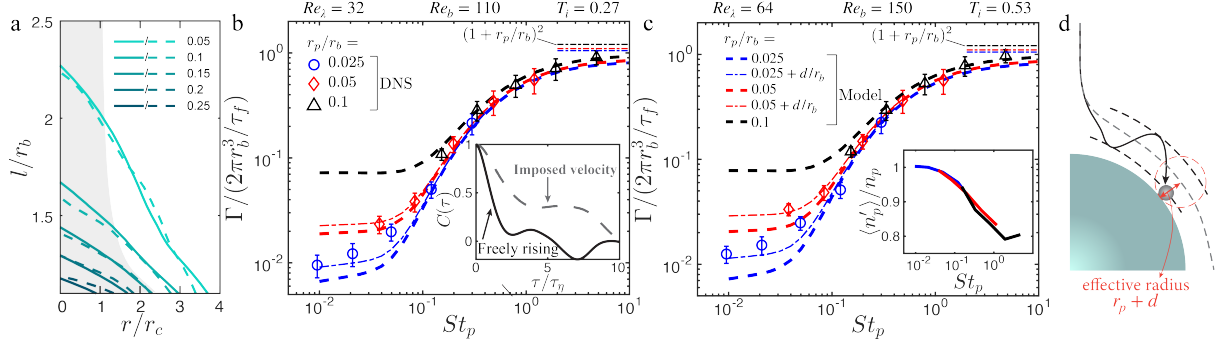


FIG. 3. (a) Contour lines of $P(r, l)$ from simulations (solid) and model (dashed lines) for $r_p/r_b = 0.05$ and $St_p = 0.04$. The grey shaded area indicates the region inside the grazing trajectory in quiescent flow. Normalized collision kernel for the freely rising bubble at (b) $Re_\lambda = 32$, $Re_b = 110$ and (c) $Re_\lambda = 64$, $Re_b = 150$. The inset in (b) compares the auto-correlation function of U'_b for the imposed velocity ($Re_\lambda = 32$, $Re_b = 120$) and freely rising bubbles ($Re_\lambda = 32$, $Re_b = 110$), respectively. The inset in (c) shows the normalized mean incoming particle density as a function of St_p at $Re_\lambda = 64$. (d) Sketch in the bubble reference frame, showing how fluctuations U'_b during the interaction effectively enlarge the particle collision radius.

of $St_p \simeq 0.1$, the contribution to collisions from fluctuating St'_p exhibits a positive bias, which explains the strongly enhanced turbulent collision rate in this range and the non-monotonic dependence on St_p . Due to the higher interceptional collision efficiency, the increase in the inertial range and hence the turbulent enhancement is less pronounced for larger size ratios r_p/r_b .

Another way to validate the model is to consider the spatial distribution of the collision probability $P(r, l) = N_c(r, l)/N(r, l)$, where r and l are distances perpendicular and along the bubble velocity direction, respectively, (see Fig. 1(c)) and $N_c(r, l)$ mea-

asures the number of colliding particles out of the total number of particles $N(r, l)$ passing through position (r, l) in a given time interval. $P(r, l)$ can be predicted from the model by superimposing the appropriate binary distributions for quiescent flow [36]. The result of doing so is again in excellent agreement with the data as shown in Fig. 3(a), confirming that the basic physical processes are well represented in the model. Consistent with Fig. 1(c), the impact of turbulence is clearly evident leading to a much wider distribution of $P(r, l)$ compared to the binary distribution in quiescent flow (grey shading).

Freely rising bubble.— Having established

the general suitability of the model to capture the relevant turbulence effects on the collision rate, we now turn to the more realistic case of a freely rising bubble. The corresponding results in terms of Γ are shown in Fig. 3(b,c) for different Re_λ . In these cases, the bubble-slip velocity pdf $f(U'_b)$ required as input for the model is obtained by measuring the fluid velocity around the bubble [36, 49].

The general agreement between Γ predicted by the model (dashed lines in Fig. 3(b,c)) and the data remains very good also for the free rising cases. Small differences arise at low St_p , where the model is found to slightly underpredict the simulation result. This can be explained by the correlation time of U'_b , which is shorter for free rising bubbles compared to the imposed velocity case (see inset in Fig. 3(b)). The resulting changes in U'_b during the bubble-particle interaction cause the particle trajectory to fluctuate in the bubble frame of reference (see Fig. 3(d)). This increases the effective collision radius of the particle to $r_p + d$, where d is a measure of the drift from the original particle trajectory. The relevant time and velocity scales for this drift are τ_f and u_η , respectively, such that $d \sim \tau_f u_\eta$ in analogy to Taylor dispersion in the ballistic regime [50]. Indeed, we find that using $d = 0.06\tau_f u_\eta$ results in good agreement with our data across different Re_λ and for different r_p , as shown by the dash-dotted lines

in Fig. 3(b,c). This effect is only relevant at $St_p \lesssim 0.1$ and becomes negligible once $r_c \gg d$ due to the inertial effect at larger St_p .

Another finding is that the incoming particle number density can differ from the global value. This is caused by clustering of bubbles and particles in different regions of the flow leading to segregation [8]. As a result $\langle n'_p \rangle / n_p$ shown in the inset of Fig. 3(c) decreases as St_p increases reaching a minimum value of about 0.8 for $St_p \approx 1$, where clustering effects are known to be strongest. The segregation effect explains why the inertial limit $(1 + r_p/r_b)^2$ at high St_p is not reached in the simulations and in the model, where this effect is accounted for.

Conclusions.—We have elucidated the relevant mechanisms governing the collision rate of inertial particles with a finite-size bubble in turbulence. We demonstrated that for the investigated practical conditions, inertial effects induced by the flow around the bubble are the dominant effect. The non-linear dependence of these effects on the bubble slip velocity leads to an increase of the collision rate in turbulence of up to 100% at $St_p \approx 0.1$ compared to quiescent flow. An additional increase in the turbulent collision rate is due to the short temporal correlation of the bubble slip velocity in the free-rising case. The effect of the resulting fluctuations during the bubble-particle interaction can be captured

by an increase in the effective collision radius of the particle and is mostly relevant in the tracer limit for $St_p \lesssim 0.1$. Segregation of bubbles and particles in turbulence reduces the particle density encountered by the bubble and hence the collision rate by up to 20% at $St_p \approx 1$. Remarkably, the effect of turbulence induced motion of the particles was found to have negligible impact on the collision process throughout. The developed frozen turbulence model provides a physically consistent framework that can be easily extended to a full collision model (by combining it with a prediction for $f(U'_b)$). The approach is also transferable to other conditions, such

as more complex shapes (by adopting a different parameterisation of E_c) and thus offers a more general relevance for collisions with finite-size objects in turbulence.

ACKNOWLEDGMENTS

We thank Timothy Chan and Duco van Buuren for fruitful discussions. This project has received funding from the European Research Council (ERC) under the European Union’s Horizon 2020 research and innovation programme (grant agreement No. 950111, BU-PACT). This work was carried out on the Dutch national e-infrastructure with the support of SURF Cooperative.

-
- [1] M. Kostoglou, T. D. Karapantsios, and O. Oikonomidou, A critical review on turbulent collision frequency/efficiency models in flotation: Unravelling the path from general coagulation to flotation, *Adv. Colloid Interface Sci.* **279**, 102158 (2020).
 - [2] A. Nguyen and H. J. Schulze, *Colloidal Science of Flotation* (CRC Press, 2003).
 - [3] B. Derjaguin and S. Dukhin, Theory of flotation of small and medium-size particles, *Prog. Surf. Sci.* **43**, 241 (1993).
 - [4] A. Pumir and M. Wilkinson, Collisional aggregation due to turbulence, *Annu. Rev. Condens. Matter Phys.* **7**, 141 (2016).
 - [5] P. G. Saffman and J. S. Turner, On the collision of drops in turbulent clouds, *J. Fluid Mech.* **1**, 16–30 (1956).
 - [6] J. Abrahamson, Collision rates of small particles in a vigorously turbulent fluid, *Chem. Eng. Sci.* **30**, 1371 (1975).
 - [7] E. Calzavarini, M. Cencini, D. Lohse, and F. Toschi, Quantifying turbulence-induced segregation of inertial particles, *Phys. Rev. Lett.* **101**, 084504 (2008).
 - [8] T. T. Chan, C. S. Ng, and D. Krug, Bubble–particle collisions in turbulence: insights from point-particle simulations, *J. Fluid Mech.* **959**, A6 (2023).

- [9] K. L. Sutherland, Physical chemistry of flotation. XI. kinetics of the flotation process, *J. Phys. Colloid Chem.* **52**, 394 (1948).
- [10] L. Flint and W. Howarth, The collision efficiency of small particles with spherical air bubbles, *Chem. Eng. Sci.* **26**, 1155 (1971).
- [11] D. A. Reay and G. A. Ratcliff, Removal of fine particles from water by dispersed air flotation: effects of bubble size and particle size on collection efficiency, *Can. J. Chem. Eng.* **51**, 178 (1973).
- [12] G. Dobby and J. Finch, Particle size dependence in flotation derived from a fundamental model of the capture process, *Int. J. Miner. Process.* **21**, 241 (1987).
- [13] R. H. Yoon and G. H. Luttrell, The effect of bubble size on fine particle flotation, *Miner. Process. Extr. Metall. Rev.* **5**, 101 (1989).
- [14] H. J. Schulze, Hydrodynamics of bubble-mineral particle collisions, *Miner. Process. Extr. Metall. Rev.* **5**, 43 (1989).
- [15] V. Sarrot, P. Guiraud, and D. Legendre, Determination of the collision frequency between bubbles and particles in flotation, *Chem. Eng. Sci.* **60**, 6107 (2005).
- [16] Z. Huang, D. Legendre, and P. Guiraud, Effect of interface contamination on particle-bubble collision, *Chem. Eng. Sci.* **68**, 1 (2012).
- [17] B. Pyke, D. Fornasiero, and J. Ralston, Bubble particle heterocoagulation under turbulent conditions, *J. Colloid Interface Sci.* **265**, 141 (2003).
- [18] A. V. Nguyen, D.-A. An-Vo, T. Tran-Cong, and G. M. Evans, A review of stochastic description of the turbulence effect on bubble-particle interactions in flotation, *Int. J. Miner. Process.* **156**, 75 (2016).
- [19] A. Hajisharifi, C. Marchioli, and A. Soldati, Particle capture by drops in turbulent flow, *Phys. Rev. Fluids* **6**, 024303 (2021).
- [20] F. Bloom and T. J. Heindel, On the structure of collision and detachment frequencies in flotation models, *Chem. Eng. Sci.* **57**, 2467 (2002).
- [21] P. Koh and M. Schwarz, Cfd modelling of bubble-particle collision rates and efficiencies in a flotation cell, *Miner. Eng.* **16**, 1055 (2003).
- [22] P. Koh and M. Schwarz, Cfd modelling of bubble-particle attachments in flotation cells, *Miner. Eng.* **19**, 619 (2006).
- [23] P. Koh and M. Schwarz, Cfd model of a self-aerating flotation cell, *Int. J. Miner. Process.* **85**, 16 (2007).
- [24] R.-H. Yoon, G. Soni, K. Huang, S. Park, and L. Pan, Development of a turbulent flotation model from first principles and its validation, *Int. J. Miner. Process.* **156**, 43 (2016).
- [25] T. Liu and M. Schwarz, Cfd-based multiscale modelling of bubble-particle colli-

- sion efficiency in a turbulent flotation cell, *Chem. Eng. Sci.* **64**, 5287 (2009).
- [26] M. Kostoglou, T. D. Karapantsios, and K. A. Matis, Modeling local flotation frequency in a turbulent flow field, *Adv. Colloid Interface Sci.* **122**, 79 (2006).
- [27] M. Kostoglou, T. D. Karapantsios, and S. Evgenidis, On a generalized framework for turbulent collision frequency models in flotation: The road from past inconsistencies to a concise algebraic expression for fine particles, *Adv. Colloid Interface Sci.* **284**, 102270 (2020).
- [28] G. Falkovich, A. Fouxon, and M. G. Stepanov, Acceleration of rain initiation by cloud turbulence, *Nature* **419**, 151 (2002).
- [29] F. Poydenot and B. Andreotti, Gap in drop collision rate between diffusive and inertial regimes explains the stability of fogs and non-precipitating clouds, *J. Fluid Mech.* **987**, A37 (2024).
- [30] T. Guillot, S. Ida, and C. W. Ormel, On the filtering and processing of dust by planetesimals-i. derivation of collision probabilities for non-drifting planetesimals, *Astron. Astrophys.* **572**, A72 (2014).
- [31] H. Homann, T. Guillot, J. Bec, C. Ormel, S. Ida, and P. Tanga, Effect of turbulence on collisions of dust particles with planetesimals in protoplanetary disks, *Astron. Astrophys.* **589**, A129 (2016).
- [32] R. S. Cushing and D. F. Lawler, Depth filtration: Fundamental investigation through three-dimensional trajectory analysis, *Environ. Sci. Technol.* **32**, 3793 (1998).
- [33] K. May and R. Clifford, The impaction of aerosol particles on cylinders, spheres, ribbons and discs, *Ann. Occup. Hyg.* **10**, 83 (1967).
- [34] J. Słomka, U. Alcolombri, E. Secchi, R. Stocker, and V. I. Fernandez, Encounter rates between bacteria and small sinking particles, *New J. Phys.* **22**, 043016 (2020).
- [35] J.-A. Arguedas-Leiva, J. Słomka, C. C. Lalescu, R. Stocker, and M. Wilczek, Elongation enhances encounter rates between phytoplankton in turbulence, *Proc. Natl. Acad. Sci.* **119**, e2203191119 (2022).
- [36] See Supplemental Material at XXX for the simulation and model details, and data of collision angle.
- [37] E. Calzavarini, Eulerian-lagrangian fluid dynamics platform: The ch4-project, *Softw. Impacts* **1**, 100002 (2019).
- [38] V. Mathai, E. Calzavarini, J. Brons, C. Sun, and D. Lohse, Microbubbles and microparticles are not faithful tracers of turbulent acceleration, *Phys. Rev. Lett.* **117**, 024501 (2016).
- [39] L. Jiang, E. Calzavarini, and C. Sun, Rotation of anisotropic particles in rayleigh-bénard turbulence, *J. Fluid Mech.*

- 901**, A8 (2020).
- [40] L. Jiang, C. Wang, S. Liu, C. Sun, and E. Calzavarini, Rotational dynamics of bottom-heavy rods in turbulence from experiments and numerical simulations, *Theor. Appl. Mech. Lett.* **11**, 100227 (2021).
- [41] Z. Liu, L. Jiang, and C. Sun, Accumulation and alignment of elongated gyrotactic swimmers in turbulence, *Phys. Fluids* **34**, 033303 (2022).
- [42] L. Jiang, C. Wang, S. Liu, C. Sun, and E. Calzavarini, Dynamics of finite-size spheroids in turbulent flow: the roles of flow structures and particle boundary layers, *J. Fluid Mech.* **939**, A22 (2022).
- [43] C. S. Peskin, The immersed boundary method, *Acta Numer.* **11**, 479 (2002).
- [44] R. Mittal and G. Iaccarino, Immersed boundary methods, *Annu. Rev. Fluid Mech.* **37**, 239 (2005).
- [45] M. Uhlmann, An immersed boundary method with direct forcing for the simulation of particulate flows, *J. Comput. Phys.* **209**, 448 (2005).
- [46] A. Wang, M. M. Hoque, G. Evans, and S. Mitra, Effect of turbulence dispersion on bubble-particle collision efficiency, *Miner. Eng.* **177**, 107374 (2022).
- [47] Z. Dai, D. Fornasiero, and J. Ralston, Particle–bubble collision models—a review, *Adv. Colloid Interface Sci.* **85**, 231 (2000).
- [48] M. Weber and D. Paddock, Interceptional and gravitational collision efficiencies for single collectors at intermediate reynolds numbers, *J. Colloid Interface Sci.* **94**, 328 (1983).
- [49] A. G. Kidanemariam, C. Chan-Braun, T. Doychev, and M. Uhlmann, Direct numerical simulation of horizontal open channel flow with finite-size, heavy particles at low solid volume fraction, *New J. Phys.* **15**, 025031 (2013).
- [50] G. I. Taylor, Diffusion by continuous movements, *Proc. London Math. Soc.* **2**, 196 (1922).